AJAB

Asian J Agric & Biol. 2024(3).
DOI: 10.35495/ajab.2023.364

Original Article

Biogenic synthesis and characterization of silver nanoparticles: exploring antioxidant and anti-Inflammatory activities and assessing antimicrobial potential against multidrug-resistant bacteria

Maria Rasool, Muhammad Hidayat Rasool*, Mohsin Khurshid, Bilal Aslam
Institute of Microbiology, Government College University Faisalabad, Faisalabad-38000, Pakistan

Received:
December 12, 2023
Accepted:
February 07, 2024
Published Online:
March 21, 2024

Abstract

Multi-drug resistant (MDR) bacterial infections significantly increase mortality, morbidity, and treatment costs when they persist. Therefore, there is a pressing need to discover, modify, or search for antimicrobial agents with the ability to combat MDR bacteria. Silver nanoparticles used in this study were synthesized by *Bacillus subtilis* and characterized through different techniques. MDR strains underwent antibacterial activity, antioxidant activity, and time-kill kinetic assays to assess susceptibility to silver nanoparticles. Furthermore, the synergistic impact of silver nanoparticles and antibiotics was examined using the two-dimensional checkerboard method to calculate the Fractional Inhibitory Concentration Index (FICI). Scanning Electron Microscopy (SEM) results revealed a circular shape of synthesized AgNPs, with an average length and area of 76.78 and 47.10 nm, respectively. UV analysis showed an optimum peak at 420 nm. XRD analysis indicated the crystalline nature of nanoparticles with diversity in size. Remarkable antioxidant potential (55% of AgNPs) was observed at a concentration of 1000 µg/ml, while minimum activity (18%) was noted at 62.6 µg/ml. Silver nanoparticles demonstrated a synergistic interaction with the antibiotic Cefixime against *Staphylococcus aureus*, *Acinetobacter baumannii*, *Escherichia coli*, and *Klebsiella pneumoniae*, with FICI values of 0.37, 0.3, 0.25, and 0.49, respectively, and an additive effect against *Pseudomonas aeruginosa*, with a FICI value of 0.7. Moreover, this research explores the anti-inflammatory potential of silver nanoparticles (AgNPs) in two distinct models: formaldehyde-induced inflammation and carrageenan-induced inflammation, along with an assessment of their in vitro anti-inflammatory activity. The findings shed light on the multifaceted role of AgNPs in mitigating inflammatory responses, offering promising avenues for therapeutic interventions.

Keywords: Green synthesis, Silver, *Bacillus subtilis*, Synergistic effect, Cefixime, XRD

How to cite this:

Rasool M, Rasool MH, Khurshid M and Aslam B. Biogenic Synthesis and Characterization of silver nanoparticles: exploring antioxidant and anti-inflammatory activities and assessing antimicrobial potential against multidrug-resistant bacteria. Asian J. Agric. Biol. 2024(3): 2023364. DOI: https://doi.org/10.35495/ajab.2023.364

*Corresponding author email:
drmhrasool@gcuf.edu.pk

This is an Open Access article distributed under the terms of the Creative Commons Attribution 4.0 License. (https://creativecommons.org/licenses/by/4.0), which permits unrestricted use, distribution, and reproduction in any medium, provided the original work is properly cited.

Introduction

Due to increasing prevalence of resistant infections, health-related problems are becoming worse worldwide in the current environment. Antimicrobial drug development has been a turning point in the fight against diseases. But the emergence of MDR bacteria makes the issue worse, making it challenging for the healthcare industry to find treatments that are effective against them (Aslam et al., 2021). Additionally, MDR bacteria have been demonstrated to form biofilms, which increase their resistance to the bacteria and decrease the drug's effectiveness. As a result, there is an urgent need for developing low-cost options for the treatment of such resistant infections, where the latest technological advancements can be employed to develop the necessary instruments and potent medications with the fewest possible hazards to society. Recently, nanotechnology has made it possible to create antimicrobial nanoparticles and delivery systems that have the potential to be used in antimicrobial treatments (Banin et al., 2017). Various nanomolecules with a range of functionalities have been developed as a result of the development of nanotechnology. Due to the numerous uses for which nanoparticles have been developed, there has been a significant growth in the hunt for them in recent decades.

Nanoparticles (NPs) are particles with a diameter minimum of 100 nm, but they have large surface area to the ratio of volume, making them highly useful in the medical field (Medina and Pieper, 2016). Because of larger surface area, stability, reactivity, and sensitivity, they are in higher demand and have applications in a variety of industries. NPs have garnered significant attention in research in recent years, with a focus on their chemical, optical, and mechanical properties. One area that has seen substantial growth between the last two decades is the use of NPs in drug delivery for therapeutic and diagnostic applications (Younas et al., 2023). The small size and efficient penetration of bacterial cells make NPs an attractive option for researchers seeking innovative ways to combat drug resistance. Furthermore, NPs possess potent antibacterial properties, making them a promising tool for fighting infections (Akram et al., 2023). Among the many types of metal nanoparticles studied in biomedicine, most popular silver nanoparticles (AgNPs) have gained attention. While exhibiting low toxicity profiles, such small particles show excellent antibacterial and antiseptic exertion against both Gram-positive and negative bacteria (Franci et al., 2015).

In the quest to synthesize AgNPs, several physical and chemical processes have explored, but nearly, there has been growing curiosity in the biological synthesis of AgNPs. This method is considered environment-friendly as it relies on the usage of safe and accepted solvents, capping, and stabilizing chemicals. Additionally, in vivo applications has discovered enhanced biocompatibility of tissue products (Figure 1). Some bacteria are capable of tolerating metal ions, making them a valuable source for nanoparticle synthesis. These bacteria are an appropriate substitute for current chemical synthesis techniques because of their unique ability to neutralize heavy metal ions (Baker et al., 2013).

Microbes could synthesize silver nanoparticles that are either intracellularly or extracellularly, but the latter method is preferred due to its simplicity. Intracellular biosynthesis occurs within living cells, such as bacteria or plant cells. These cells uptake metal ions and employ intracellular processes to transform these ions into nanoparticles. The cell's biochemical machinery, which includes enzymes and cellular organelles, plays a pivotal role in facilitating this transformation. On the other hand, extracellular biosynthesis takes place outside the cell, either in the external environment or in the extracellular matrix. Microorganisms, like bacteria or fungi, often participate in extracellular biosynthesis. They release enzymes or metabolites that interact with metal ions in the surrounding environment, ultimately resulting in the formation of nanoparticles (Lahiri et al., 2021). The downstream processing for the release and collection of nanoparticles from biomass is economically feasible without requiring any additional processes (Hulkoti and Taranath, 2014). Moreover, microbial enzymes do a crucial role in establishing extracellular bio reduction, which requires effective electron transport. Specifically, the nitrate reductase enzyme has been found to be efficient in converting nitrate to nitrite by transmitting an electron to the silver ion, thus enabling the extracellular synthesis of silver nanoparticles (Figure 2) (Prabhu and Poulose, 2012). Furthermore, organic functional groups within microbial cell walls have been identified as playing a role in bio-reduction, employing a non-enzymatic reducing mechanism to synthesize silver nanoparticles (AgNPs). This research aims to

synthesize AgNPs using Bacillus subtilis strains, followed by employing various spectroscopy and microscopy techniques to characterize the resulting nanoparticles. Additionally, the study investigates the antibacterial and antioxidant properties of the synthesized AgNPs against multi-drug resistant (MDR) pathogenic bacterial strains.

Material and Methods

Bacterial source

The Institute of Microbiology, Government College University Faisalabad, Pakistan, provided *Bacillus subtilis*, which had already been characterized by 16S rRNA amplification and sequencing. Bacterial culture was sub-cultured on Nutrient agar (Oxoid, UK) to maintain the viability overtime.

Metal resistivity test

Metal resistivity of the *B. subtilis* strain was checked by using silver nitrate as the major source of silver metal. Colonies were grown on nutrient agar in the presence of AgNO3 (1mM sterilized- filtered AgNO3 solution was dissolved into the medium before it solidified, and then allowed to cool). The bacteria were allowed to grow on enriched agar after solidification. The selected strain for nanoparticle synthesis was the one that grew on the enriched agar (Tariq et al., 2020).

Biomass production and extracellular biosynthesis of AgNPs

For biomass production, 100 ml of nutrient media was inoculated with 1 µL of bacterial culture in a conical flask and incubated at 37° centigrade under shaking incubator at speed of 150 rpm for 24 hours. After 24 hours, the growth of bacteria was observed and centrifuged the culture at 10,000 rpm for about 10 minutes. Supernatant was collected and placed it in a clean conical flask in preparation for the next step (Tariq et al., 2020). To synthesize silver nanoparticles, bacterial supernatant solution was mixed with a sterile silver nitrate solution. The mixture was placed under a light environment at 37 °C for 24 hours, shaking at a speed of 150 rpm. After 24 hours, reduction of silver ions to the silver atoms was observed. The change in color of the AgNPs (from pale yellow to deep brown) served as a visual indicator of their extracellular synthesis (Alsamhary, 2020). Control tests were also done by using silver nitrate mixture and the media as positive and negative controls, respectively. The reaction mixture and control samples were subjected to identical environmental conditions.

Characterization of AgNPs

UV-Vis analysis

Double-beam UH5300 UV-VIS absorption spectrophotometer was used for the confirmation of nanoparticle synthesis (Bastús et al., 2016). The spectrum range was adjusted in between 300–700 nm region. A blank reference was utilized to adjust the spectra's baseline. The "OriginPro 8.5" program (OriginLab, Northampton, Massachusetts, USA) was used to plot the absorption graph.

Electron microscopy

Transmission and scanning electron microscopy were used to determine the size and structure of the synthesized nanoparticles, as described previously (Mohanta et al., 2017). The surface morphology was measured using Scanning Electron Microscopy (SEM) at a magnifying power of 10000 (Shu et al., 2020).

FTIR analysis

A FTIR spectrophotometer was used to determine the functional groups of the biomolecules that are in the charge of dissolving silver nanoparticles. The powdered form of AgNPs was subjected to Fourier transform infrared spectroscopy. The resulting data was plotted and analyzed using the software "OriginPro 8.5" (Sathyavathi et al., 2011).

XRD analysis

The chemical makeup of the biosynthesized silver nanoparticles was accessed using energy-dispersive X-ray (EDX) analyzer (JEOL model JSM-6380 LA, Tokyo, Japan) (Shu et al., 2020). Graphite monochromatic-equipped Shimadzu XRD model 6000 diffractometer (Japan) was promoted to analyze the crystallographic properties of the biosynthesized AgNPs. As previously reported, the analysis was conducted at 1.540A wavelength and voltage of 40 kV (Qais et al., 2019).

Differential scanning calorimetry (DSC) and thermogravimetric analysis (TGA)

The thermal properties of both silver nitrate and

silver nanoparticles (NPs) were examined using a DSC calorimeter and TGA analyzer for comprehensive thermal studies.

Antibacterial activity screening against MDR bacterial species

Multidrug-resistant strains of both Gram-positive and Gram-negative bacteria were obtained from the culture bank of the Institute of Microbiology at Government College University, Faisalabad. Confirmatory tests such as API (Analytical Profile Index), the VITEK 2 system, and molecular characterization with species-specific primers were also done. Antibacterial efficacy of synthesized silver nanoparticles against MDR strains was assessed by using the following methods.

Agar well assay was used to evaluate the antibacterial properties of AgNPs against Gram-positive and Gram-negative MDR bacterial strains. Bacterial suspensions containing 10^8 CFU/ml from 18 to 24-hour-old cultures were prepared and the viability was confirmed by measuring their optical density (OD) at 600 nm, ranging from 0.06-0.08. Using a cotton swab, the bacterial lawn was prepared using sterilized MH agar plates. The AgNPs with varying concentrations (1000 g/ml, 2000 g/ml, and 3000 g/ml) were loaded uniformly (100µl) into each of the 6 mm-diameter wells formed by the sterile steel borer. The plates were incubated at 37 °C for 24 hours and the diameter of inhibitory zone was determined (Hungund et al., 2015). DMSO solution was used as negative control.

The MIC of the synthesized AgNPs was calculated using the agar well diffusion technique in line with a prior study's guidelines (Patra and Baek, 2016). AgNPs were serially diluted twice from the solution in MH broth for the test (1000 g/ml, 500 g/ml, 250 g/ml, 125 g/ml, 62.5 g/ml, 31.25 g/ml, 15.63 g/ml, 7.81 g/ml, 3.90 g/ml, and 1.95 g/ml). Microbial suspension in broth served as the positive control, and sterile MH broth as the negative control. Parafilm was employed to seal the plate and then incubated for 24 hours at 37 °C. The well's opacity in which no growth was observed was recorded as MIC.

MBC shows the lowest concentration of an antibiotic that can kill microorganisms. 100 µL of contents from the wells of the microtiter plate were taken and placed on sterilized LB Agar plates. After 24 to 48 hours incubation, plates with no growth were identified as having the minimum bacterial concentration (Ibrahim, 2015).

Growth curve was analyzed by taking periodic optical density measurements (600 nm) of the bacterial cultures incubated with and without nanoparticles.

Antioxidant activities of AgNPs

Silver nanoparticles were assessed for in vitro antioxidant activity using radical scavenging tests, including 1,1-diphenyl-2-picrylthydrazyl, hydrogen peroxide (H2O2), and ferric reducing antioxidant power. The concentrations of silver nanoparticles and the standard solution (ascorbic acid) ranged from 1000 to 62.6 µg/ml. Spectrophotometry was employed to calculate the absorbance of the solutions relative to the corresponding blank solution. The 1,1-diphenyl-2- picryl-hydrazyl test was utilized to determine antioxidant activity (Sowndhararajan and Kang, 2013). Additionally, using butylated hydroxytoluene (BHT) as a standard, optical density was measured at 517 nm, and the results were presented as a percentage of radical scavenging activity.

The antioxidant capacity of AgNPs was calculated using the protocol of (Sylvie et al., 2014) and the absorbance of mixture was reported at 700 nm. The scavenging activity of different concentrations of silver nanoparticles (AgNPs) on hydroxyl radicals was assessed following the protocol (Jayaprakasha et al., 2004). The intensity of the reaction mixture was measured at 230 nm, and the hydroxyl radical assay results were expressed as a percentage of antioxidant activity, with ascorbic acid serving as the standard.

Time-kill kinetic assay

Time-kill kinetic studies of silver nanoparticles (AgNPs) were conducted following the established protocol with slight modifications (Lau et al., 2014). Individual colonies of bacterial strains were obtained from overnight cultured plates and suspended in sterilized LB broth to achieve a density corresponding to 0.5 McFarland standards. The death curves of *S. aureus*, *E. coli*, *K. pneumoniae*, *P. aeruginosa*, and *A. baumannii* were analyzed at time intervals of 0, 2, 4, 8, and 24 hours, with varying amounts of NPs (0, 0.5 MIC, 1 MIC, 2 MIC, 4 MIC, respectively, for each strain). At each time point, 100 µl of suspensions was pipetted and plated on LB agar to enumerate the colony-forming units (CFU/ml). The plated cells were then incubated at 37˚C±2 for 1 day, and the killing rate was represented graphically by plotting viable cells (CFU/ml) against time.

Evaluation of the synergistic impact of AgNPs & the antibiotic Cefixime

To evaluate the synergistic impact of the antibiotic Cefixime and AgNPs against MDR strains, a two-dimensional checkerboard method was used to calculate the Fractional Inhibitory Concentration Index (Reyes-Torres et al., 2019). The checkerboard method was carried out on 96-well plate.

Anti-inflammatory activity

The experiment adhered to the protocol published (Helfand et al., 1982). In a 96-well plate, diluted whole blood in Hanks' Balanced Salt Solution (HBSS) (25 µL) was incubated in triplicate with varying doses of silver nanoparticles (AgNPs) ranging from 1 to 100 µg/mL. Control wells were filled only with HBSS and cells (blood phagocytes). The plate was then incubated at 37ºC for 15 minutes in the thermostat chamber of a luminometer. In addition to the control wells containing HBSS, each well received 25 µL of serum opsonized zymosan and 25 µL of luminol. Ibuprofen served as the standard, and the level of reactive oxygen species was quantified.

***In vivo* assay for anti-inflammatory activity**

A total of 36 Wistar rats divided in 6 groups (each group contain 6 Wistar rats) with 200-250 g body weight were employed for the in vivo experiment. The animals were housed in standard laboratory conditions, maintaining a temperature of 23 ± 2°C, 60% humidity, and a 12-hour day-and-night cycle. They were provided unrestricted access to food and water for two weeks prior to the commencement of the experiment. The Government College University Faisalabad, Pakistan, Animal Ethics Committee gave its approval for the experiment before it could be carried out (GCUF/ERC/03).

Carrageenan induced inflammation model

The protective effect of AgNPs against inflammation was assessed using an animal model of acute inflammation induced by carrageenan. Acute irritation was induced by sub-plantar injection of 0.1 mL of 1% w/v carrageenan in normal saline into the left hind paw of rat. Nine groups, each consisting of five animals, were randomly assigned.

Group I: The control group received 1 mL/kg of vehicle solvent.

Group II: Carrageenan injection was administered as a disease control measure. Group III: The standard group received a 10 mg/kg dosage of diclofenac.

AgNPs were orally administered to Groups IV, V, and VI at doses of 25, 75, and 125 mg/kg, respectively. All groups (II–VI) received a 0.1 mL (1%) carrageenan injection, except for the control group.

Rat's hind paw edema was measured using a digital Vernier caliper over six consecutive hours. To calculate percentage inhibition, the following formula was implemented: (Li et al., 2019).

$$\text{Percentage of inhibition (\%)} = \frac{(Kt - Ko)\text{disease control} - (Kt - Ko)\text{treated}}{(Kt - Ko)\text{disease control}} \times 100$$

Formaldehyde induced chronic inflammation model

The application of a low dose of formalin to the rat's hind paw induced neurogenic inflammation mediated by substances such as histamine, prostanoids, and neuropeptides. The inhibitory impact of AgNPs on formalin-induced inflammation was determined following the previously outlined technique (Fu et al., 2001).

Group I served as the control group, receiving neither carrageenan nor an injection of 1 mL/kg of distilled water. Group II, the standard medication treatment group, received an oral dosage of 10 mg/kg diclofenac. Group III was the inflammation model group, receiving a formaldehyde injection.

Groups IV, V, and VI received oral dosages of 25, 75, and 125 mg/kg of AgNPs, respectively. Except for the control group, all groups (II–VI) received a formaldehyde injection of 0.02 ml at a 2% v/v.

The treatment period lasted for twelve days. On the twelfth day, animals were subjected to an overnight fast. Following anesthesia, blood was drawn into heparinized tubes via heart puncture, and ketamine hydrochloride (24 mg/kg) was used for hematological and biochemical examination.

Table-1. List of primers with their product size

Genes	Sequence 5 ->3	Primer	Product size (bp)	Accession No.
IL-1α (Interleukin-1 alpha)	CCTCGTCCTAAG TCACTCG	Forward	102	NM_017019.1
	GGCTGGTTCCAC TAGGCTTT	Reverse		
IL-1 β (Interleukin-1beta)	GACTTCACCATG GAACCCGT	Forward	104	NM_031512.2
	GGAGACTGCCCA TTCTCGAC	Reverse		
TNF α (Tumor necrosis factor-alpha)	GGAGGGAGAACA GCAACTCC	Forward	168	NM_012675.3
	TCTGCCAGTTCC ACATCTCG	Reverse		
GADPH (Glyceraldehyde 3-phosphate dehydrogenase)	GGAGTCCCCATC CCAACTCA	Forward	173	XM_017592435.1
	GCCCATAACCCC CACAACAC	Reverse		

Quantification of inflammatory biomarkers by qPCR

Using real-time qPCR, the mRNA expression levels of inflammatory cytokines were evaluated. Table 1 contains the primer list and the corresponding product sizes for each primer. The Trizol technique was used to extract RNA from blood samples, and a cDNA synthesis kit was used to create cDNA. The first denaturation was conducted for five minutes at 95°C. Thereafter, there were forty cycles of denaturation for fifteen seconds at 95°C, annealing for twenty seconds at 60°C, and extension for twenty seconds at 72°C. The determination of inflammatory biomarker gene expression was conducted by means of GADPH as an internal reference.

Estimation of inflammatory biomarkers by ELISA

After the 12-day formaldehyde treatment was over, the Elabscience kit (Houston, Texas, USA) was used to measure the levels of tumor necrosis factor-α and nterleukin-6 in the serum.

Estimation of biochemical and hematological parameters

Following the administration of anesthesia, blood samples were obtained by heart puncture at the conclusion of the formaldehyde-induced chronic inflammation experimental investigation. Using commercially available kits and following the manufacturer's protocol, the levels of bilirubin, alanine transaminase (ALT), aspartate transaminase (AST), alkaline phosphatase, gamma glutamate, total proteins, albumin, and globulin were measured.

Histopathological analysis

After anesthesia was administered, blood samples were taken by cardiac puncture at the end of the formaldehyde-induced chronic inflammation experiment. The levels of bilirubin, albumin, globulin, alkaline phosphatase, gamma glutamate, alanine transaminase (ALT), aspartate transaminase (AST), total proteins, and gamma glutamate were determined using commercially available kits and according to the manufacturer's procedure.

Tissue antioxidant enzymes

Using a thiobarbituric acid (TBA) standard curve, the previously used approach was used to assess the level of malondialdehyde (MDA) in the liver homogenate (Saleem et al., 2021b). The breakdown of hydrogen peroxide was used to measure catalase activity, which was then computed using a method from a prior (Roy et al., 2005). The tissue homogenate was combined with nitroblue tetrazolium, phenazine methosulphate, and Triton X to measure the activity of superoxide dismutase. Glacial acetic acid was added to stop the reaction, and the activity was reported in units/mL. Using a previously reported approach employing sodium azide and 5,5-dithio bis-nitrobenzoic acid, the amount of glutathione peroxidase was measured and expressed as µmol of

glutathione oxidized per minute per mg of protein. Furthermore, the decreased glutathione level (Saleem et al., 2021a).

Statistical analysis

Three times per experiment were run, and SPSS and GraphPad Prism were utilized for analyzing the data.

Results

Synthesis and characterization of silver nanoparticles

A change in appearance of color from yellow to deep brown acted as visible proof for AgNPs synthesis. To obtain a higher yield, the silver nanoparticles were optimized at different concentrations of silver nitrate (1mM, 2mM, 3mM, 5mM, 10mM, and 20mM). The absorbance spectra of all samples were studied and recorded in the wavelength range of 300-700 nm with highest absorption peak at 420nm and at a concentration of 10mM silver nitrate solution.

Transmission Electron Microscopy (TEM) and Scanning Electron Microscopy (SEM) analysis

TEM analysis was used to determine the topographical information of the produced AgNPs. At low magnification power, TEM micrographs revealed that the synthesized silver nanoparticles were nearly round in shape and present in clusters, as shown in Figure 1.

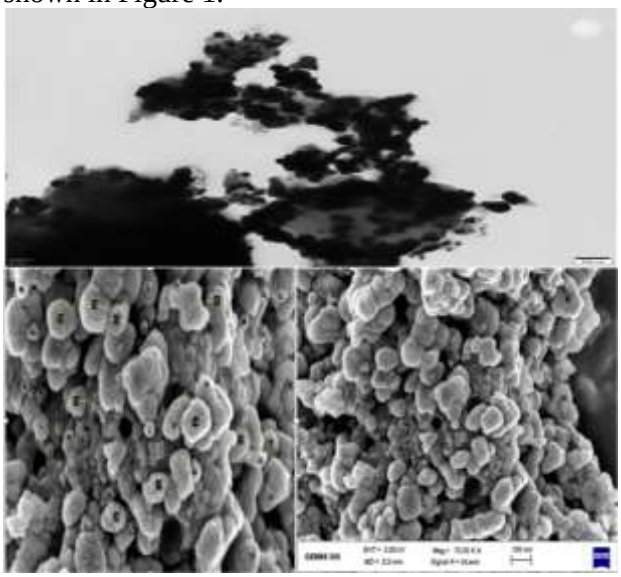

Figure-1. TEM (top) and SEM (bottom) micrograph of *B. subtilis* synthesized AgNPs

Scanning electron microscopy was used to determine the surface morphological structure of the AgNPs synthesized from *Bacillus subtilis*. Silver nitrate was placed into a solution, and the mixture was spread onto a slide to create SEM plates. A thin film of platinum was then coated on the slide to enhance conductivity. The prepared slides were scanned at a 3.00 kV accelerating voltage, and high-quality magnification images were captured as shown in Figure 1. The average sizes of the nanoparticles were showed using ImageJ software, and the results revealed that the average area and length of the *B. subtilis* synthesized AgNPs were 76.78 and 47.10, respectively.

FTIR, XRD and thermal studies

FTIR spectroscopy was used to analyze the functional groups that were already present on the surface of the synthesized AgNPs. The resulting spectra determined a broad-spectrum peak at 3420 cm^{-1}, which is associated with O-H and N-H vibrations. The peak observed at 2918 cm^{-1} showed Asymmetrical and symmetrical stretching of CH2, while the peak at 2850 cm^{-1} was related to CH3 symmetric stretching. A sharp peak shift was observed between 1690 cm^{-1} and 1630 cm^{-1}, indicating C=O stretching and the presence of an aliphatic group of amides. Finally, a peak was reported at 1060 cm^{-1}, showing the presence of a carboxylic chain shown in Figure 2A.

To confirm that AgNPs were made entirely of one material, an XRD measurement was made. As indicated by Figure 2B, diffraction peaks 2θ appear at 38.1°, 44.18°, 64.35°, and 78.23°, corresponding to (111), (200), (220), and (311) planes. All these peaks indicate that nanoparticles are diverse in size but crystalline in nature.

The DSC curve of silver nitrate displayed endothermic peaks at 197 °C and 387 °C, as illustrated in Figure 2C. In contrast, the NPs exhibited an endothermic peak at 213 °C and an exothermic peak at 301 °C. The TGA curve of silver nitrate indicated the onset of weight loss at 115°C, with a 72% weight loss observed at 500°C. In comparison, the NPs exhibited weight loss starting at 289 °C, and a 90% weight loss was observed at 500 °C, as depicted in Figure 2D.

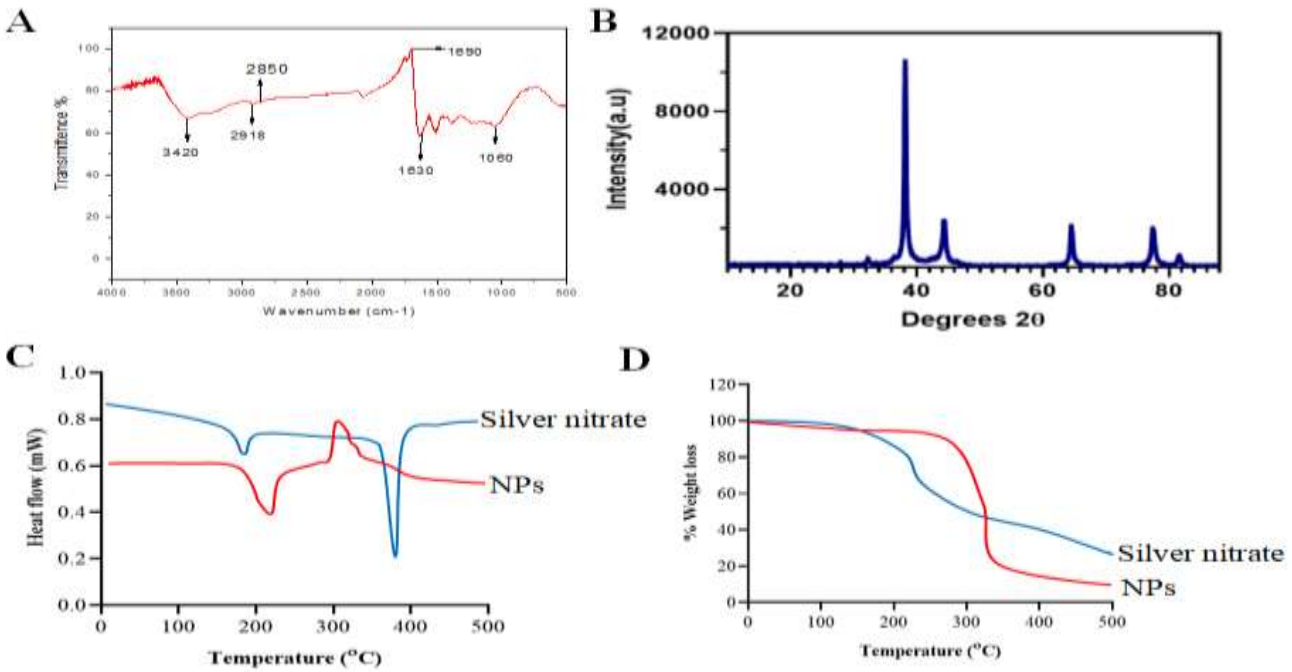

Figure-2. A) FTIR spectrum of *B. subtilis* synthesized AgNPs (B) XDR pattern of *B. subtilis* synthesized AgNPs (C) DSC (D) and TGA of silver nitrate and NPs.

Antimicrobial efficacy of AgNPs

Results of agar-well diffusion assay revealed that *B. subtilis*-synthesized AgNPs have promising antibacterial activity against MDR Gram-positive and Gram-negative bacteria, including *S. aureus* (MRSA), *P. aeruginosa, A. baumannii, E. coli, and K. pneumoniae*. To evaluate the antibacterial activity, the zones of inhibition were measured. Different concentrations of AgNPs i.e., 2000 µg/ml, 1000 µg/ml, 500 µg/ml, and 250 µg/ml (prepared in DMSO), were used against these pathogenic MDR bacteria. The maximum zone of inhibition (28 mm) was measured at 2000 µg/ml against *K. pneumoniae*, whereas the minimum zone of inhibition (16 mm) at 250 µg/ml against *A. baumannii* as.

Using the conventional micro broth dilution technique, values of a minimum inhibitory concentration of synthesized AgNPs were measured and are also concise in Table 2. The MIC rate of synthesized AgNPs versus five species of highly pathogenic MDR Gram-positive and Gram – negative bacteria revealed a maximum antimicrobial efficacy, i.e., (500µg/ml) for *P. aeruginosa* and *A. baumannii*, (250 µg/ml) for *S. aureus* and *K. pneumoniae*. On the other side, the minimum antimicrobial efficacy (125 µg/ml) was measured for *E. coli*.

Table-2. Minimum bactericidal concentration values of prepared AgNPs for selected MDR bacteria

Selected MDR strains	MIC (µg/ml)	MBC (µg/ml)
Staphylococcus aureus	250	500
Pseudomonas aeruginosa	500	1000
Acinetobacter baumannii	500	1000
Escherichia coli	125	250
Klebsiella pneumoniae	250	500

The microtiter dilution technique was used to determine the minimum bactericidal concentration of the five isolates that had been chosen. The results of MBC are reported in Table 2. The results revealed that bactericidal activity ranged from 1000-250 µg/ml. The maximum bactericidal activity was observed at 1000 µg/ml by *P. aeruginosa* and *A. baumannii*. The minimum bactericidal activity was shown at 250 µg/ml by *E. coli* and *K. pneumoniae.*

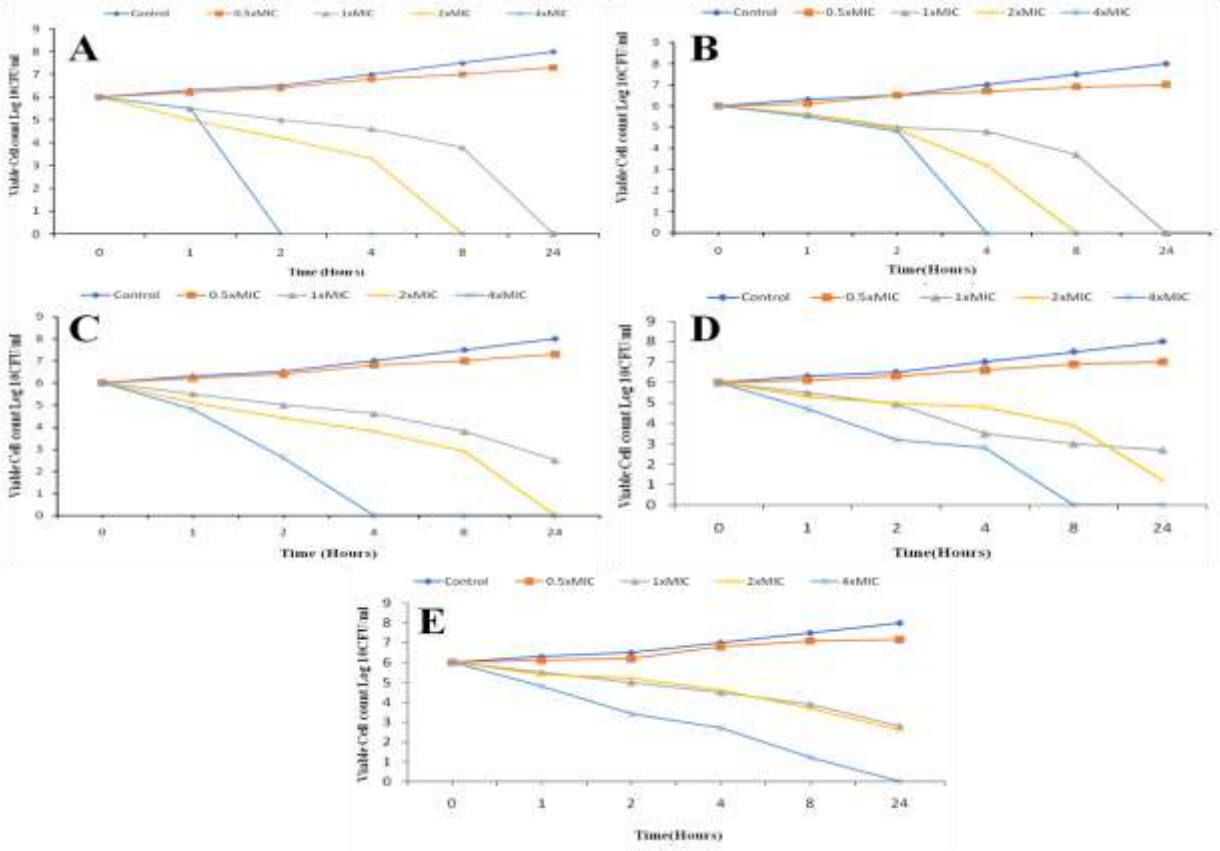

Figure-3. Time kill kinetic activities of AgNPs against A) *E. coli* B) *S. aureus* C) *K. pneumoniae* D) *P. aeruginosa* E) *A. baumannii* at different concentrations and time length.

Time kill kinetic assay

A time-kill kinetic assay was employed to further investigate the killing effect of AgNPs by using different concentrations (0 MIC, 0.5 MIC, 1 MIC, 2 MIC, and 4 MIC) of NPs at many different time intervals (0, 1, 2, 4, 8, and 24 hours). The viable cell count (log10) of control cells continuously increased with time, while the cell count of cells treated with sub-inhibitory concentrations of AgNPs also gradually increased with time, but not as much as in control cells. The reduction in bacterial cell count was dose dependent. The bactericidal endpoint was met for *E. coli* and *S. aureus* after 4 hours of fermentation at 2 MIC (3.3 and 3.2 g/ml, respectively); however, the endpoint was attained quicker after 1 and 2 hours at 4 MIC (5.5 and 4.8 g/ml, respectively). After 8 hours at 2 MIC (2.9 g/ml) and after 2 hours at 4 MIC (2.6 g/ml), *K. pneumoniae* bacteria were eliminated. At 4 MIC (2.8 and 1.2 g/ml, respectively), the bactericidal action of AgNPs in *P. aeruginosa* and *A. baumannii* was observed after 4 and 8 h as shown in Figure-3.

Synergistic studies

The synergistic impact of AgNPs combined with the selected antibiotic (Cefixime) was determined by the conventional checkerboard 2-dimensional method using broth micro dilution technique, and the FIC index was calculated by assessing the degree of interaction between AgNPs and the selected antibiotic against all bacterial isolates, as shown in Table 3. To determine the MIC of selected antibiotic combined with AgNPs, redox nitro-blue tetrazolium chloride dye was used. The change of color from yellow to blue indicates viable cells, and no color change revealed the absence of viable cells. As shown in Table 3, AgNPs exhibited synergistic interaction with Cefixime against *S. aureus*, *A. baumannii*, *E. coli*, and *K. pneumoniae* with FICI values of 0.37, 0.3, 0.25, and 0.49, respectively. Whereas AgNPs showed an additive effect with Cefixime against *P. aeruginosa* with a FICI value of 0.7.

Table-3: Synergistic effect of Cefixime and AgNPs against different bacteria

Selected MDR strains	MIC		FICI
	Cefixime	AgNPs	
A. baumannii	250	500	0.3(S)
E. coli	250	125	0.25 (S)
K. pneumoniae	125	250	0.49 (S)
P. aeruginosa	500	500	0.7 (A)
S. aureus	250	250	0.37 (S)

Fractional inhibitory concentration index (FICI), synergistic effect (S), antagonistic effect (A)

Antioxidant Activities

Antioxidants swiftly scavenge DPPH, a stable radical with much amount of absorption at 517 nm. This method has been frequently employed to find reducing agents and the behavior of free radicals. The minimal activity (18 %) was tested at a concentration of 62.6 g/ml, while the exceptional antioxidant potential (55 % of AgNPs) was assessed at a concentration of 1000 g/ml as shown in Figure 4A. AgNPs had powerful antioxidant capabilities, and nanoparticles significantly boosted their ability to decrease DPPH free radicals in a concentration-dependent manner.

Since reducing power is a strong sign of exceptional antioxidant activity, antioxidants may be understood as inhibiting oxidants and reductants. In this assay, the highest antioxidative activity (59 %) was exhibited at a concentration of 1000 µg/ml of AgNPs, and the minimum activity (24%) was observed at 62.6 µg/ml, revealing dose-dependent antioxidant activity of NPs mentioned in Figure 4B. FRAP assay results at concentrations of 1000, 500, 250, 125, and 62.6 % of AgNPs were 59, 46, 33, 25, and 24 %, respectively.

OH radicals has high reactivity that allows them to interact with a wide range of molecules, scavenging them is a crucial antioxidant actions like amino acids, nucleotides, sugars, and lipids found in cells. So, the removal of hydroxyl radicals is necessary to protect living systems. It has been shown that the scavenging activity of AgNPs increased with increasing sample concentrations shown in Figure 4C and was found in the range of 13 to 52 %.

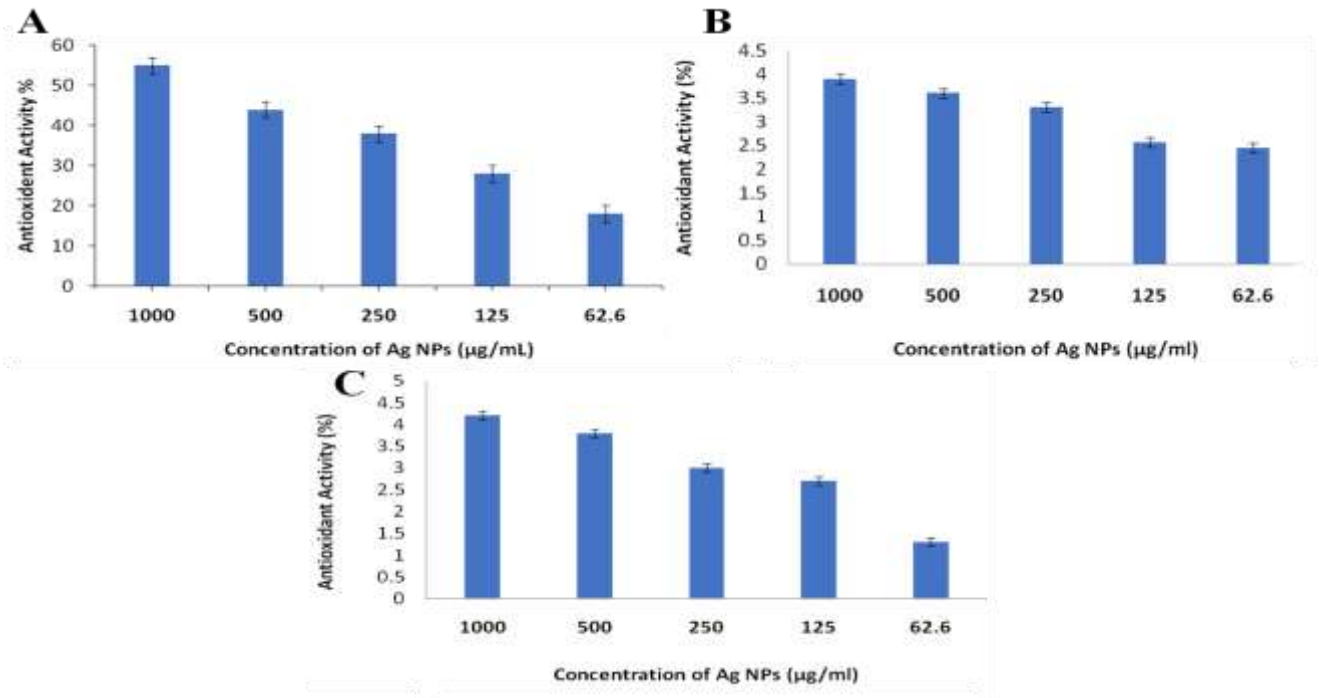

Figure-4. Antioxidant activities of synthesized AgNPs via A) DPPH B) FRAP C) H_2O_2 scavenging assays at various concentrations.

Anti-inflammatory activity of AgNPs

In a dose-dependent manner, silver nanoparticles (AgNPs) ranging from 1 to 100 µg/ml showed inhibition of inflammation. At 100 µg/mL, AgNPs (IC50=12±0.01µg/mL) demonstrated 76% inhibition, while ibuprofen (IC50 = 10 ± 0.01 µg/mL) demonstrated 79% (Table 4).

Table-4. Effect of AgNPs against protein denaturation by using bovine serum albumin

Sample (µg/mL)	% of inhibition	IC50 ± SD
Ibuprofen		
100	79	
25	62	
10	46	10 ± 0.01
1	5	
AgNPs		
100	75.5	
25	69	
10	44	12 ± 0.11
1	11	

When paw inflammation was compared to a carrageenan-induced inflammatory paradigm in rats, AgNPs demonstrated a significant ($p < 0.001$) reduction in inflammation of paw (Figure 5). At dosages of 25, 75, and 125 mg/kg, AgNPs demonstrated a significant percentage of inhibition (Figure 6).

When compared to the formaldehyde-induced inflammation paradigm, AgNPs demonstrated a considerable ($p < 0.001$) anti-inflammatory potential against the inflammation of the left hind paw caused by formaldehyde (Table 5). When compared to formaldehyde treatment groups, AgNPs at dose levels of 25, 75, and 125 mg/kg dose-dependently reduced paw inflammation in a manner similar to that of diclofenac (Figure 6).

AgNPs on liver function parameters

The formaldehyde treatment group had noticeably higher levels of rheumatoid factor, alkaline phosphatase, and C-reactive protein. When compared to the formaldehyde-induced inflammation group, the treatment with AgNPs significantly ($p < 0.05$) reduced these parameters in the treated groups. In comparison to the control group, it was shown that formaldehyde significantly ($p < 0.001$) raised the levels of ALT and AST in the inflammatory model group. The restoration of ALT and AST levels was dose-dependent and showed signs of Diclofenac and AgNPs recovery ($p < 0.001$). Alkaline phosphatase (ALP) was also higher in the inflammatory model group than in the control due to formaldehyde. Figure 7 shows the dose-dependent response seen by the AgNPs-treated groups.

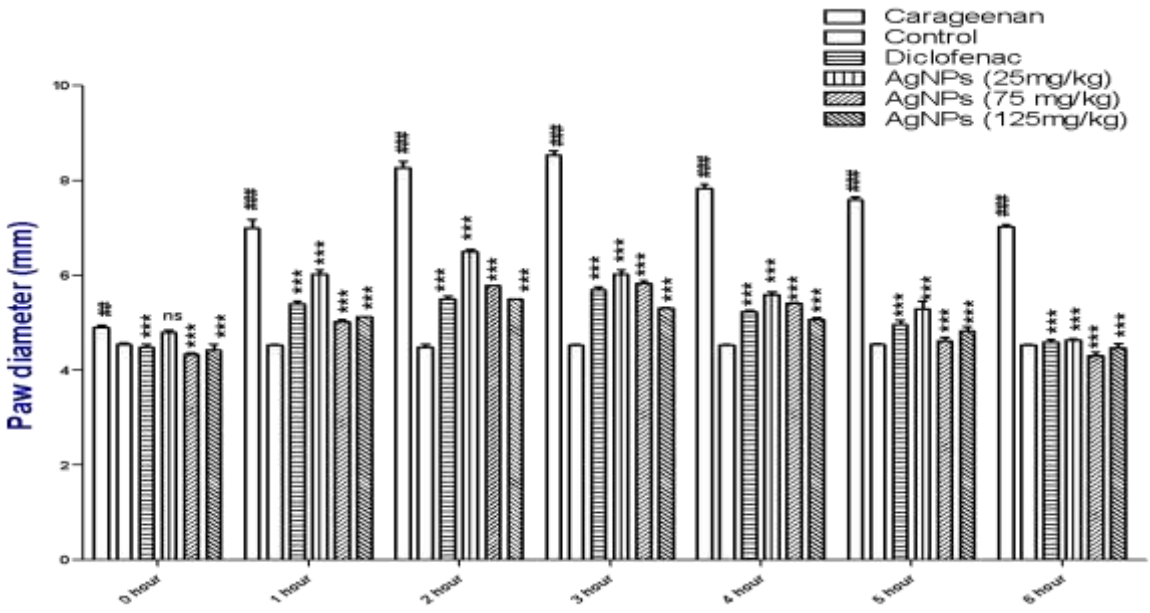

Figure-5. Effect of AgNPs on paw edema (mm) in rats

*** $p < 0.001$, and ns (non-significant) relative to the inflammatory model produced by carrageenan, ### $p < 0.001$ compared to control

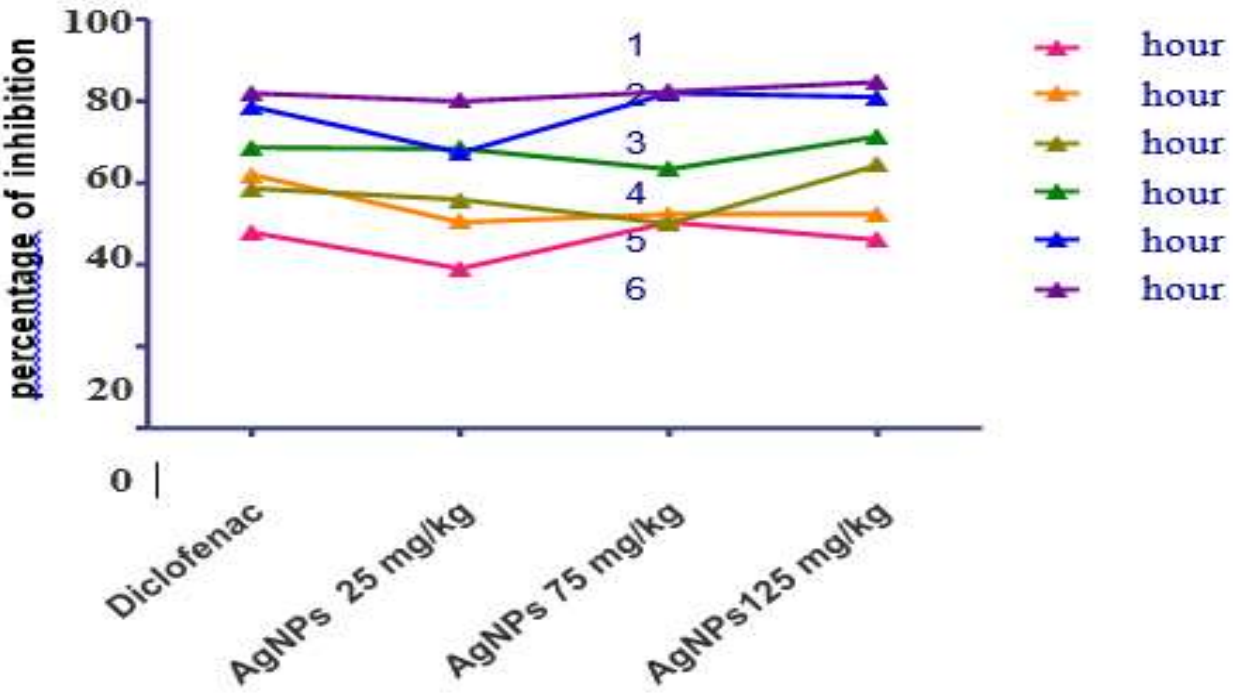

Figure-6: AgNPs' impact on the percentage of inhibition of paw edema caused by carrageenan

Table-5. AgNPs' anti-inflammatory effects on paw edema caused by formaldehyde (mm).

Treatment groups	Day 1	day 3	day 5	day 9	day 12
Control	5.04 ±0.21***	5.07 ± 0.01***	5.09 ± 0.01***	5.12 ± 0.01***	5.18± 0.01***
Formaldehyde	8.3 ± 0.05	7.7±0.02	8.4± 0.09	7.8±0.06	7.3±0.01
Diclofenac	6.3 ± 0.11***	6.64 ± 0.11***	7.6±0.04***	7.0±0.02***	6.7±0.13***
AgNPs 25mg/kg	6.69 ± 0.01***	6.7± 0.02***	6.54 ± 0.07***	6.30±0.02***	5.99±0.2***
AgNPs 75 mg/kg	6.54 ±0.21***	6.46 ± 0.17***	6.38± 0.21***	6.37±0.06***	5.94±0.02***
AgNPs 125mg/kg	6.61 ±0.11***	6.29 ± 0.18***	6.26± 0.13***	6.07±0.06***	5.97±0.03***

*** $p < 0.001$ and ns (non-significant) relative to the inflammatory model produced by formaldehyde

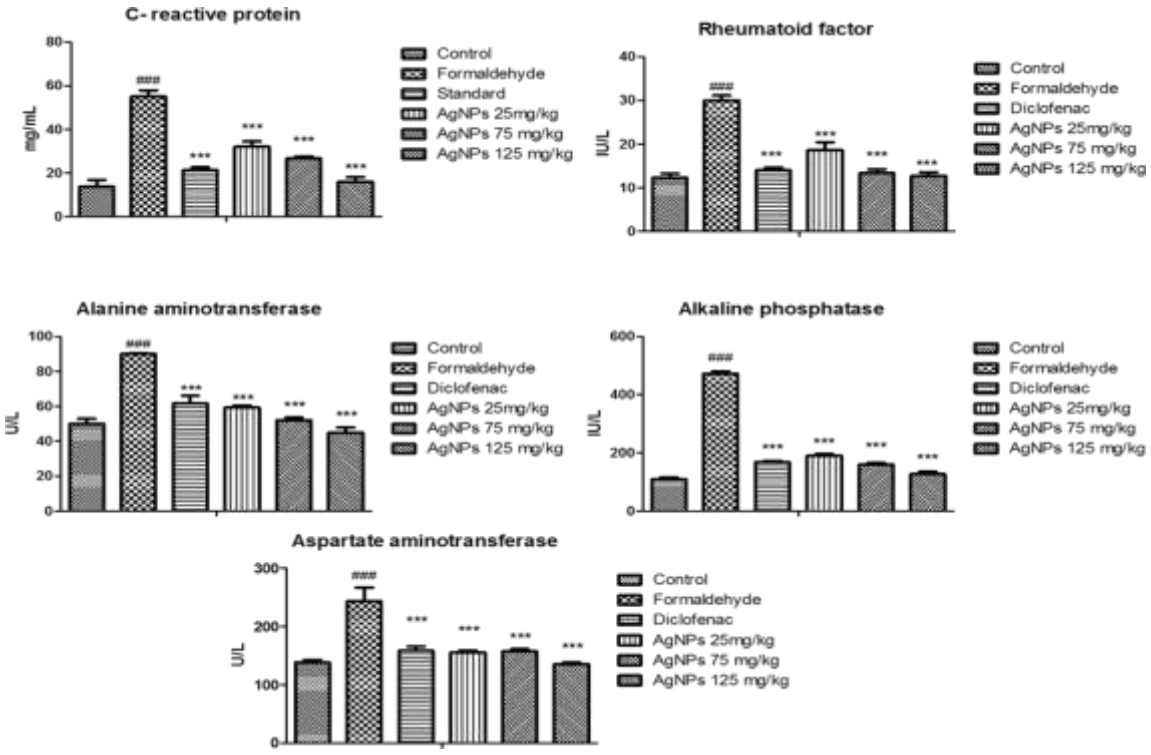

Figure-7. Effect of AgNPs on C-reactive protein.
Values are examined using one way ANOVA and expressed as mean±SEM. ### compared to the control group, *** (P< 0.001), **(P<0.01) and *(P<0.05) compared to the disease control.

Serum concentration of inflammation markers

In the inflammatory model treated with formaldehyde, there was a considerable increase in the levels of interleukin-6 and tumor necrosis factor-α. But in contrast to the formaldehyde-treated group, the higher levels of these biomarkers were reduced in a dose-dependent manner by both the treatment with AgNPs and the treatment with diclofenac (Figure 8 & 9).

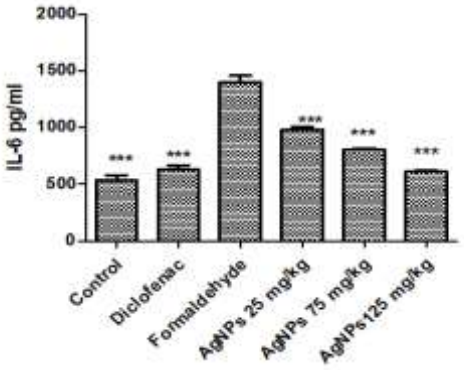

Figure-8. Effect of AgNPs on serum concentration of IL-6. * *p < 0.001* was considered as significant**

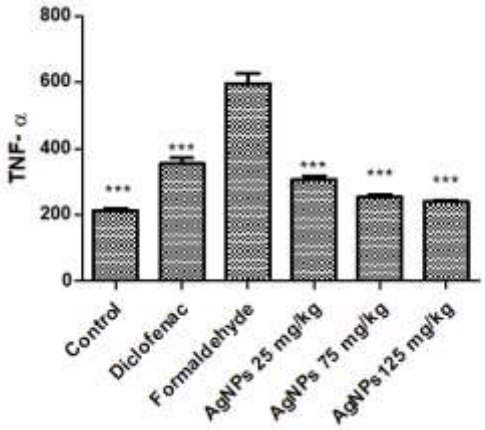

Figure-9. Effect of AgNPs on serum concentration of TNF-α. * *p < 0.001* as significant.**

Antioxidant parameters in formaldehyde induced inflammation model

When compared to control and other treatment groups, formaldehyde significantly decreased ($p < 0.05$) the level of first line antioxidant enzymes in the inflammation model group (Table 6). The groups treated with formaldehyde showed a significant ($p < 0.05$) increase in lipid peroxidation when compared

to the control group that received AgNPs therapy. AgNPs and the reference medication, diclofenac, significantly ($p < 0.05$) increased the enzyme level in a dose-dependent manner.

Histological studies

The dermis and epidermis of the normal control group showed no lesions and a normal appearance, according to a histopathological investigation of the skin tissues from the paws. However, the application of formaldehyde to rat paws caused inflammation, which resulted in a significant neutrophil infiltration. As seen in Figure 10, AgNPs significantly decreased cellular infiltrates and extravasation in treated mice as compared to the formaldehyde inflammatory model group.

Table-6. Effect of AgNPs on antioxidant parameters

Groups	CAT (IU/µL)	SOD (IU/µL)	MDA (TBA mg/mL)	GSH (µ/mg protein)	GPx (µ/mg protein)
Control	0.88± 0.05	0.1± 0.01	60.11±0.02	0.80 ± 1.1	11.01± 1.01
Formaldehyde treated group (Disease control)	$0.7\pm0.02^{***}$	$0.035\pm0.031^{***}$	$82.01\pm0.14^{***}$	$0.3\pm 0.01^{***}$	$5.30 \pm 0.11^{***}$
Diclofenac	0.83 ± 0.01^{ns}	0.07 ± 0.13^{ns}	75.01 ± 0.11^{ns}	0.73 ± 0.21^{ns}	9.34 ± 0.21^{ns}
AgNPs 25mg/kg	0.74 ± 0.12^{ns}	$0.04\pm0.014^{***}$	70.12 ± 0.12^{ns}	$0.4\pm0.15^{***}$	$4.23\pm0.11^{***}$
AgNPs 75 mg/kg	0.61 ± 0.3^{ns}	$0.05 \pm0.19^{***}$	$64.27\pm0.01^{***}$	$0.55\pm0.19^{***}$	$7.12\pm0.2^{***}$
AgNPs 125mg/kg	0.67 ± 0.11^{ns}	0.08 ± 0.12^{ns}	$65.23\pm0.14^{***}$	0.76 ± 0.12^{ns}	10.03 ± 0.13^{ns}

*** $p < 0.001$ and ns (non-significant) relative to the inflammatory model caused by formaldehyde

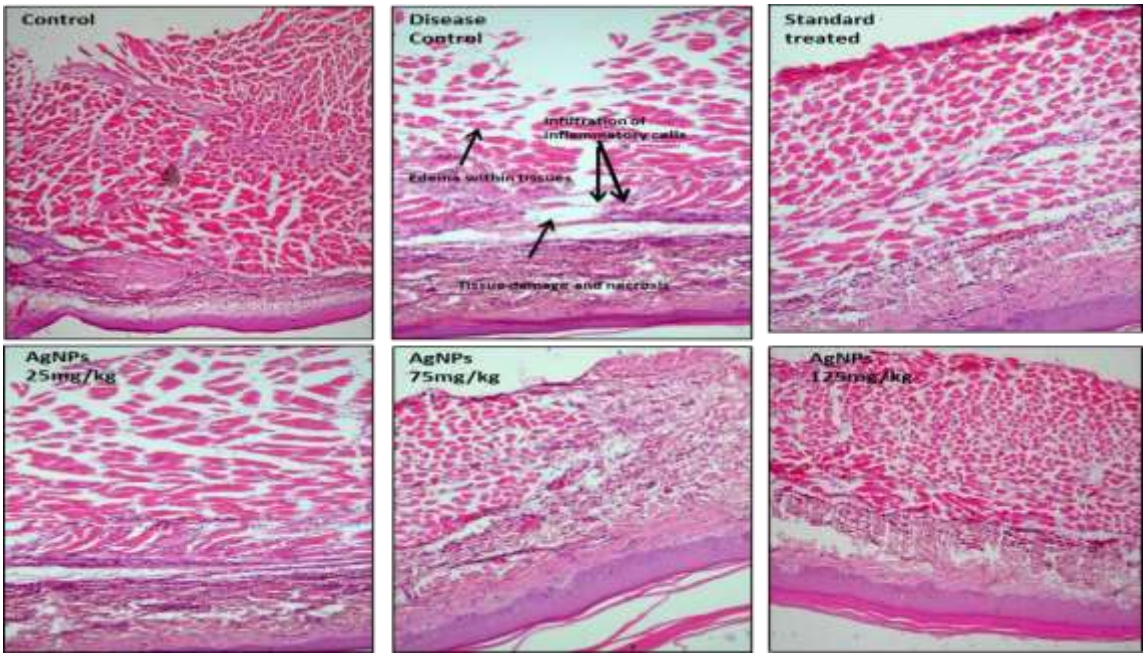

Figure-10. AgNPs' impact on the histopathology of the rat paw following formaldehyde treatment. Disease control (group treated with diclofenac) and standard treatment (group treated with formaldehyde inflammatory model).

Discussion

Synthesis of silver nanoparticles using bacterial culture was initially identified by the appearance of a distinct brown color of reaction mixture. Further studies have shown that this color is due to the surface Plasmon vibrations of the nanoparticles serves as a spectroscopic indicator of their production (Abdeen et al., 2014). This color change is caused by the transformation of silver ions into silver atoms in the presence of an aqueous enzymatic extraction from the cell culture supernatant. Formation of silver atoms with brownish appearance has been proposed to be greatly aided by enzymes and reaction intermediates like nitrate reductase. Research has shown that proteins and enzymes in the culture supernatant are the responsible factors for producing AgNPs.

To measure the deep brown color change, absorbance was measured at a specific wavelength, and the absorption spectra were compiled. The sample exhibited a wide range of resonance at nearly 410-450 nm, indicating the accumulation of AgNPs. The peak at 410 nm corresponds to Plasmon transfer vibration, while the peak at 450 nm was attributed to excited longitudinal Plasmon vibration.

TEM analysis was performed to confirm morphology of biogenic AgNPs, which were found amorphous in nature. Produced AgNPs were slightly rounded, with average size ranged from 47.10 to 76.78. These biologically produced AgNPs have the potential for use in several medical treatments, such as microbial elimination with the help of UV irradiation and optical probes for medical diagnosis via visible emission, as described in the previous studies (Zhang et al., 2016). This data can be easily compared with previously recorded data using *B. subtilis* (PTCC 1023) culture supernatant and the fungus *Candida albicans* (PTCC 5011) culture supernatant. The prospect of synthesizing AgNPs through a biogenic approach offers new opportunities for large-scale, economical, and eco- friendly production of controlled shaped bio-nanomaterials.

FTIR analysis revealed the presence of an amine group and a carboxylic acid derivative within protein compounds in the infrared portion of the electromagnetic spectrum. The wave number 3237 cm^{-1} stretching indicates the presence of O-H functional groups with H-bonds, and the wave number's bending indicates the presence of N-H functional groups. Alkane C-H stretching vibration was thought to be the cause of the band at 2927 cm^{-1}. A possible cause of C=O stretching is the presence of the carbonyl group. The aromatic ring C=C stretching vibration was responsible for the peak at 1625 cm^{-1}. The C-H bending was what caused the peak to be 1383 cm^{-1}. Additionally, the peaks at 1235 and 1069 cm^{-1} were attributed to C-N stretching, possibly as a result of the presence of an amine group. The aromatic ring was characterized by another strong band at 832 cm^{-1} (Ahmed et al., 2015).

The existence of protein in the clear filtrate was ensured by the amino acid peaks observed in the UV-vis spectral analysis. The peak's wavelength changed (by a blue or red shift), which may have been caused by nanoparticles of various sizes and shapes. At their particular wavelength, each of the synthesized nanoparticles showed only one peak showing their round shape {Panda, 2021 #43. A study suggests that nanoparticles and proteins can interact through the enzymatic attraction of carboxylic groups or free amine groups. Therefore, it is suggested that protein molecules released outside the microbial cell help stabilize these silver nanoparticles in the aqueous medium.

AgNPs have four distinct peaks, which correspond to the (111), (200), (220), and (311) planes, according to XRD research. The presence of peaks at different positions is consistent with many earlier studies on the synthesis of AgNPs from bacilli, fungi, or plants. Different previous studies observed peaks at the same degree, and the data confirmed the crystalline effect of AgNPs with a size of 21.5 nm. It is suggested that the sharp peaks may be due to a capping agent that stabilizes the AgNPs, while a few unassigned peaks may be caused by the biomolecule crystallizing on the surface of the AgNPs (Sreelekha et al., 2021).

Bacterially synthesized silver nanoparticles (AgNPs) are very effective against five species of multi-drug-resistant (MDR) bacteria. These AgNPs release silver ions, which combine with nucleic acids, carbohydrates, proteins, and lipids on the bacterial cell walls to create a cavity that penetrates the plasma membrane and eventually enters the cytoplasm (Bruna et al., 2021). Some studies suggest that AgNPs may interfere with the electron transport chain of microbes or connect with the microbial plasma membrane, disrupting the permeability process or respiratory activities of cells. Additionally, AgNPs can enter microbial cells by passing through their plasma membranes (Sharma et al., 2009). One study suggests that positively charged AgNPs can

attract negatively charged membranes of highly pathogenic MDR bacteria, contributing to their antimicrobial potential (Vijayakumar et al., 2013). Free radicals of silver metal produced by AgNPs increase the production rate of highly reactive oxygen species by increasing oxidation forces, causing the rupture of microbial nucleic acids and membranes and resulting in cell death. Another study revealed that the release of silver ions by AgNPs accounted for their antimicrobial efficacy (Feng et al., 2000).

In the present study, the maximum zone of inhibition (28mm) was determined at 2000µg/ml against *K. pneumoniae*, whereas the minimum zone of inhibition (16mm) was measured at 250µg/ml against *baumannii*, which is consistent with various studies (Younas et al., 2023; Abootalebi et al., 2021). In present study, the MIC of synthesized AgNPs versus five species of highly pathogenic MDR Gram-positive and Gram-negative bacteria revealed a maximum antimicrobial efficacy, i.e., (500µg/ml) for *P. aeruginosa* and *A. baumannii*, (250µg/ml) for *S. aureus* and *K. pneumoniae*. However, the current study revealed minimum antimicrobial efficacy (125µg/ml) for *E. coli*. It might occur as a result of the existence of other substances with antibacterial capabilities, such as deoxyviolacein, oxyviolacein, FK228 and others (Abootalebi et al., 2021). Even at high concentrations, chemically created nanoparticles had a slight growth- inhibitory effect. Thus, it was found that biologically synthesized AgNPs were the most efficient growth inhibitors of MDR bacteria (Khanal et al., 2022).

The remarkable antioxidant potential (55 % of AgNPs) was assessed at a different amount concentration of 1000 µg/ml, while the minimum activity (18 %) was examined at 62.6µg/ml. FRAP assay results at concentrations of 1000, 500, 250, 125, and 62.6 % of AgNPs were 59, 46, 33, 25, and 24 %, respectively. It has been shown that the scavenging activity of AgNPs increased with increasing sample concentrations and was found in the range of 13 to 52 %. These results are better than different previous studies (Khanal et al., 2022). The reduction in bacterial cell count was dose- dependent. The bactericidal endpoint for *E. coli* and *S. aureus* was attained after 4 hours of incubation at 2 MIC (3.3 and 3.2 g/ml, respectively); however, the endpoint was reached more quickly after 1 and 2 hours at 4 MIC (5.5 and 4.8 g/ml, respectively). At 2 MIC (2.9 g/ml) after 8 hours and at 4 MIC (2.6 g/ml) after 2 hours, *K. pneumoniae* bacteria had been eliminated. The bactericidal effect of AgNPs for *P. aeruginosa* and *A. baumannii* was reached after 4 and 8 h at 4 MIC (2.8 and 1.2 µg/ml, respectively). Silver nanoparticles were successful in our investigation at preventing bacterial proliferation influenced by dosage and time. AgNPs may prevent both bacterial growth and reproduction, according to the growth curves of bacteria exposed to them (Loo et al., 2018). In the current investigation, the bacterial cells were effectively eliminated after 4 to 8 hours of nanoparticle therapy. AgNPs exhibited synergistic interaction with Cefixime against *S. aureus*, *A. baumannii*, *E. coli*, and *K. pneumoniae*, with FICI values of 0.37, 0.3, 0.25, and 0.49, respectively. Whereas AgNPs showed an additive effect with Cefixime against *P. aeruginosa* with a FICI value of 0.7. Instead of finding novel medications and avoiding the toxicity of synthetic compounds, mixing antibiotics with nanoparticles was an attractive option for restoring the action of antibiotic at the smallest possible dose. (Esmaili and Hosseini Doust, 2019) concluded in their research that AgNPs increased the antibacterial activity of Cefixime when both were used in combination. The best synergistic effect was observed when both were mixed equally at their MIC level. Overall, biologically synthesized silver nanoparticles exhibited robust antimicrobial activity against an array of drug- resistant bacterial strains, indicating that they may be exploited as an alternative source of antimicrobial agents for both Gram-positive as well as Gram-negative bacteria. The current research explores the anti-inflammatory potential of silver nanoparticles (AgNPs) in two distinct models: formaldehyde-induced inflammation and carrageenan-induced inflammation.

Additionally, the study includes an assessment of their in vitro anti-inflammatory activity. The findings illuminate the multifaceted role of AgNPs in mitigating inflammatory responses, providing promising avenues for therapeutic interventions (Younas et al., 2023). The observed suppression of inflammation in the formaldehyde-induced model highlights the potential of AgNPs as effective agents in combating inflammation triggered by environmental pollutants. The reduction in pro-inflammatory markers and modulation of inflammatory mediators following AgNP treatment suggest their ability to intervene in pathways associated with formaldehyde-induced inflammation (Younas et al., 2023). Notably, the mechanism by which AgNPs exert their anti- inflammatory effects

in this context warrants further exploration to elucidate their specific interactions and molecular targets. Similarly, the reduction of inflammation in the carrageenan-induced model strengthens the evidence for the anti-inflammatory properties of AgNPs (Younas et al., 2023). The noteworthy decrease in edema formation and the suppression of inflammatory cytokines following AgNP administration underscore their potential as therapeutic agents in acute inflammatory conditions. The precise mechanisms underlying their action in this model merit detailed investigation to delineate the pathways modulated by AgNPs during carrageenan-induced inflammation. The in vitro assessment of AgNPs for their anti-inflammatory activity offers additional insights into their potential mechanisms of action (Choi et al., 2021). The demonstrated ability to inhibit the release of pro-inflammatory mediators, including cytokines and chemokines, from immune cells suggests a direct influence on inflammatory cascades at a cellular level (Choi et al., 2021). These findings support the notion that AgNPs may exert their anti-inflammatory effects by interfering with inflammatory signaling pathways or by regulating immune cell function. The multifaceted anti-inflammatory effects of AgNPs observed across different models and in vitro settings hold promise for diverse therapeutic applications [56]. However, several critical aspects necessitate further exploration. Elucidating the precise molecular mechanisms underlying the anti- inflammatory action (Abootalebi et al., 2021) of AgNPs is imperative to optimize their efficacy and safety profiles. Additionally, comprehensive investigations into the long-term effects, potential toxicity, and biodistribution of AgNPs are essential for their translational potential as therapeutic agents.

Conclusion

Biologically synthesized silver nanoparticles have exhibited robust antimicrobial and antioxidant properties against multiple drug-resistant bacterial strains, suggesting their potential as potent antimicrobial agents effective against both Gram-negative and Gram-positive bacteria. Furthermore, the presented findings emphasize the notable anti-inflammatory properties of AgNPs in formaldehyde-induced and carrageenan-induced inflammation models, complemented by their demonstrated in vitro activity. These results underscore AgNPs as promising candidates for the development of novel anti-inflammatory therapies. To fully harness the therapeutic potential of AgNPs in managing inflammatory disorders, further research endeavors are crucial. Investigating mechanistic insights and safety profiles will provide essential knowledge for the comprehensive understanding and optimization of AgNPs as effective therapeutic agents.

Disclaimer: None.
Conflict of Interest: None.
Source of Funding: This study was funded by the internal funds of Institute of Microbiology, Government College University Faisalabad, Pakistan and no external funding was availed.

Contribution of Authors

Rasool M: Conducted the study, compilation of data and manuscript write up
Rasool MH: Conceptualization of study and supervision of research work
Khurshid M: Technical assistance in Manuscript write up and proof reading
Aslam B: Technical assistance in tabulation, figures, graphs and data analysis

References

Abdeen S, Geo S, Praseetha P and Dhanya R, 2014. Biosynthesis of silver nanoparticles from Actinomycetes for therapeutic applications. Int. J. Nano Dimens. 5: 155-162. https://doi.org/10.7508/IJND.2014.02.008

Abootalebi SN, Mousavi SM, Hashemi SA, Shorafa E, Omidifar N and Gholami A, 2021. Antibacterial effects of green-synthesized silver nanoparticles using Ferula asafoetida against Acinetobacter baumannii isolated from the hospital environment and assessment of their cytotoxicity on the human cell lines. J. Nanomater. 2021: 1-12. https://doi.org/10.1155/2021/6676555

Ahmed MJ, Murtaza G, Mehmood A and Bhatti TM, 2015. Green synthesis of silver nanoparticles using leaves extract of Skimmia laureola: characterization and antibacterial activity. Mater. Lett. 153: 10-13. https://doi.org/10.1016/j.matlet.2015.03.143

Akram K, Khan I, Rehman A, Hayat A, Rehman

MU, Khurshid M, Hayat P, Alshammari A, Alharbi M and Massa S, 2023. Exploring the antimicrobial potential of biologically synthesized zero valent iron nanoparticles. Open Chem. 21. https://doi.org/doi:10.1515/chem-2022-0355

Alsamhary KI, 2020. Eco-friendly synthesis of silver nanoparticles by Bacillus subtilis and their antibacterial activity. Saudi J. Biol. Sci. 27: 2185-2191. https://doi.org/10.1016/j.sjbs.2020.04.026

Aslam B, Khurshid M, Arshad MI, Muzammil S, Rasool M, Yasmeen N, Shah T, Chaudhry TH, Rasool MH, Shahid A, Xueshan X and Baloch Z, 2021. Antibiotic Resistance: One Health One World Outlook. Front. Cell. Infect. Microbiol. 11: 771510. https://doi.org/10.3389/fcimb.2021.771510

Baker S, Harini B, Rakshith D and Satish S, 2013. Marine microbes: invisible nanofactories. J. Pharm. Res. 6: 383-388. https://doi.org/10.1016/j.jopr.2013.03.001

Banin E, Hughes D and Kuipers OP, 2017. Bacterial pathogens, antibiotics and antibiotic resistance. FEMS Microbiol. Rev. 41: 450-452. https://doi.org/10.1093/femsre/fux016

Bastús NG, Piella J and Puntes V, 2016. Quantifying the sensitivity of multipolar (dipolar, quadrupolar, and octapolar) surface plasmon resonances in silver nanoparticles: The effect of size, composition, and surface coating. Langmuir 32: 290-300. https://doi.org/10.1021/acs.langmuir.5b03859

Bruna T, Maldonado-Bravo F, Jara P and Caro N, 2021. Silver Nanoparticles and Their Antibacterial Applications. Int. J. Mol. Sci. 22. https://doi.org/10.3390/ijms22137202

Choi JS, Jung HC, Baek YJ, Kim BY, Lee MW, Kim HD and Kim SW, 2021. Antibacterial activity of green-synthesized silver nanoparticles using Areca catechu extract against antibiotic-resistant bacteria. Nanomaterials 11: 205. https://doi.org/10.3390/nano11010205

Esmaili S and Hosseini Doust R, 2019. Synergistic effect of silver nanoparticles (AgNPs) and gentamicin against clinical isolates of Pseudomona aeruginosa. Medical Science Journal of Islamic Azad Univesity-Tehran Medical Branch 29: 64-70.

Feng QL, Wu J, Chen GQ, Cui F, Kim T and Kim J, 2000. A mechanistic study of the antibacterial effect of silver ions on Escherichia coli and Staphylococcus aureus. J. Biomed. Mater. Res. 52: 662-668. https://doi.org/10.1002/1097-4636(20001215)52:4

Franci G, Falanga A, Galdiero S, Palomba L, Rai M, Morelli G and Galdiero M, 2015. Silver nanoparticles as potential antibacterial agents. Molecules 20: 8856-8874. https://doi.org/10.3390/molecules20058856

Fu K-Y, Light AR and Maixner W, 2001. Long-lasting inflammation and long-term hyperalgesia after subcutaneous formalin injection into the rat hindpaw. J. Pain 2: 2-11. https://doi.org/10.1054/jpai.2001.9804

Helfand SL, Werkmeister J and Roder JC, 1982. Chemiluminescence response of human natural killer cells. I. The relationship between target cell binding, chemiluminescence, and cytolysis. J. Exp. Med. 156: 492-505. https://doi.org/10.1084/jem.156.2.492

Hulkoti NI and Taranath T, 2014. Biosynthesis of nanoparticles using microbes—a review. Colloids Surf. B Biointerfaces 121: 474-483. https://doi.org/10.1016/j.colsurfb.2014.05.027

Hungund BS, Dhulappanavar GR and Ayachit NH, 2015. Comparative evaluation of antibacterial activity of silver nanoparticles biosynthesized using fruit juices. J. Nanomed. Nanotechnol. 6: 1. https://doi.org/10.4172/2157-7439.1000271

Ibrahim HM, 2015. Green synthesis and characterization of silver nanoparticles using banana peel extract and their antimicrobial activity against representative microorganisms. J. Radiat. Res. Appl. Sci. 8: 265-275. https://doi.org/10.1016/j.jrras.2015.01.007

Jayaprakasha GK, Rao LJ and Sakariah KK, 2004. Antioxidant activities of flavidin in different in vitro model systems. Bioorg. Med. Chem. 12: 5141-5146. https://doi.org/10.1016/j.bmc.2004.07.028

Khanal LN, Sharma KR, Paudyal H, Parajuli K, Dahal B, Ganga G, Pokharel YR and Kalauni SK, 2022. Green synthesis of silver nanoparticles from root extracts of Rubus ellipticus Sm. and comparison of antioxidant and antibacterial activity. J. Nanomater. 2022: 1-11. https://doi.org/10.1155/2022/1832587

Lahiri D, Nag M, Sheikh HI, Sarkar T, Edinur HA, Pati S and Ray RR, 2021. Microbiologically-Synthesized Nanoparticles and Their Role in Silencing the Biofilm Signaling Cascade. Front.

Microbiol. 12: 636588. 10.3389/fmicb.2021.636588

Lau K, Zainin N, Abas F and Rukayadi Y, 2014. Antibacterial and sporicidal activity of Eugenia polyantha Wight against Bacillus cereus and Bacillus subtilis. Int. J. Curr. Microbiol. Appl. Sci. 3: 499-510.

Li C-L, Tan L-H, Wang Y-F, Luo C-D, Chen H-B, Lu Q, Li Y-C, Yang X-B, Chen J-N and Liu Y-H, 2019. Comparison of anti-inflammatory effects of berberine, and its natural oxidative and reduced derivatives from Rhizoma Coptidis in vitro and in vivo. Phytomedicine 52: 272-283. https://doi.org/10.1016/j.phymed.2018.09.228

Loo YY, Rukayadi Y, Nor-Khaizura M-a-R, Kuan CH, Chieng BW, Nishibuchi M and Radu S, 2018. In vitro antimicrobial activity of green synthesized silver nanoparticles against selected gram-negative foodborne pathogens. Front. Microbiol. 9: 1555. https://doi.org/10.3389/fmicb.2018.01555

Medina E and Pieper DH, 2016. Tackling threats and future problems of multidrug-resistant bacteria. Curr. Top. Microbiol. Immunol. 398: 3-33. https://doi.org/10.1007/82_2016_492

Mohanta YK, Panda SK, Jayabalan R, Sharma N, Bastia AK and Mohanta TK, 2017. Antimicrobial, antioxidant and cytotoxic activity of silver nanoparticles synthesized by leaf extract of Erythrina suberosa (Roxb.). Front. Mol. Biosci. 4: 14. https://doi.org/10.3389/fmolb.2017.00014

Patra JK and Baek KH, 2016. Biosynthesis of silver nanoparticles using aqueous extract of silky hairs of corn and investigation of its antibacterial and anticandidal synergistic activity and antioxidant potential. IET Nanobiotechnol. 10: 326-333. https://doi.org/10.1049/iet-nbt.2015.0102

Prabhu S and Poulose EK, 2012. Silver nanoparticles: mechanism of antimicrobial action, synthesis, medical applications, and toxicity effects. Int. Nano Lett. 2: 1-10. https://doi.org/10.1186/2228-5326-2-32

Qais FA, Shafiq A, Khan HM, Husain FM, Khan RA, Alenazi B, Alsalme A and Ahmad I, 2019. Antibacterial effect of silver nanoparticles synthesized using Murraya koenigii (L.) against multidrug-resistant pathogens. Bioinorg. Chem. Appl. 2019. https://doi.org/10.1155/2019/4649506

Reyes-Torres MA, Mendoza-Mendoza E, Miranda-Hernández ÁM, Pérez-Díaz MA, López-Carrizales M, Peralta-Rodríguez RD, Sánchez-Sánchez R and Martinez-Gutierrez F, 2019. Synthesis of CuO and ZnO nanoparticles by a novel green route: antimicrobial activity, cytotoxic effects and their synergism with ampicillin. Ceram. Int. 45: 24461-24468. https://doi.org/10.1016/j.ceramint.2019.08.171

Roy S, Sehgal R, Padhy B and Kumar V, 2005. Antioxidant and protective effect of latex of Calotropis procera against alloxan-induced diabetes in rats. J. Ethnopharmacol. 102: 470-473. https://doi.org/10.1016/j.jep.2005.06.026

Saleem U, Akhtar R, Anwar F, Shah MA, Chaudary Z, Ayaz M and Ahmad B, 2021a. Neuroprotective potential of Malva neglecta is mediated via down-regulation of cholinesterase and modulation of oxidative stress markers. Metab. Brain Dis. 1-12. https://doi.org/10.1007/s11011-021-00683-x

Saleem U, Shehzad A, Shah S, Raza Z, Shah MA, Bibi S, Chauhdary Z and Ahmad B, 2021b. Antiparkinsonian activity of Cucurbita pepo seeds along with possible underlying mechanism. Metab. Brain Dis. 1-21. https://doi.org/10.1007/s11011-021-00707-6

Sathyavathi R, Krishna M and Rao DN, 2011. Biosynthesis of silver nanoparticles using Moringa oleifera leaf extract and its application to optical limiting. J. Nanosci. Nanotechnol. 11: 2031-2035. https://doi.org/10.1166/jnn.2011.3581

Sharma VK, Yngard RA and Lin Y, 2009. Silver nanoparticles: green synthesis and their antimicrobial activities. Adv. Colloid Interface Sci. 145: 83-96. https://doi.org/10.1016/j.cis.2008.09.002

Shu M, He F, Li Z, Zhu X, Ma Y, Zhou Z, Yang Z, Gao F and Zeng M, 2020. Biosynthesis and antibacterial activity of silver nanoparticles using yeast extract as reducing and capping agents. Nanoscale Res. Lett. 15: 1-9. https://doi.org/10.1186/s11671-019-3244-z

Sowndhararajan K and Kang SC, 2013. Free radical scavenging activity from different extracts of leaves of Bauhinia vahlii Wight & Arn. Saudi J. Biol. Sci. 20: 319-325. https://doi.org/10.1016/j.sjbs.2012.12.005

Sreelekha E, George B, Shyam A, Sajina N and Mathew B, 2021. A Comparative Study on the Synthesis, Characterization, and Antioxidant

Activity of Green and Chemically Synthesized Silver Nanoparticles. BioNanoScience 11: 489-496. https://doi.org/10.1007/s12668-021-00824-7

Sylvie DD, Anatole PC, Cabral BP and Veronique PB, 2014. Comparison of in vitro antioxidant properties of extracts from three plants used for medical purpose in Cameroon: Acalypha racemosa, Garcinia lucida and Hymenocardia lyrata. Asian Pac. J. Trop. Biomed. 4: S625-S632. https://doi.org/10.12980/APJTB.4.201414B168

Tariq F, Ahmed N, Afzal M, Khan MaU and Zeshan B, 2020. Synthesis, Characterization and antimicrobial activity of Bacillus subtilis-derived silver nanoparticles against multidrug-resistant bacteria. Jundishapur J. Microbiol. 13. https://doi.org/10.5812/jjm.91934

Vijayakumar M, Priya K, Nancy F, Noorlidah A and Ahmed A, 2013. Biosynthesis, characterisation and anti-bacterial effect of plant-mediated silver nanoparticles using Artemisia nilagirica. Ind. Crops Prod. 41: 235-240. https://doi.org/10.1016/j.indcrop.2012.04.017

Younas M, Rasool MH, Khurshid M, Khan A, Nawaz MZ, Ahmad I and Lakhan MN, 2023. Moringa oleifera leaf extract mediated green synthesis of silver nanoparticles and their antibacterial effect against selected gram-negative strains. Biochem. Syst. Ecol. 107: 104605. https://doi.org/10.1016/j.bse.2023.104605

Zhang X-F, Liu Z-G, Shen W and Gurunathan S, 2016. Silver nanoparticles: synthesis, characterization, properties, applications, and therapeutic approaches. Int. J. Mol. Sci. 17: 1534. https://doi.org/10.3390/ijms17091534